Electron and nuclear dynamics following ionisation of modified bismethylene-adamantane†

Morgane Vacher,* Fabio E. A. Albertani, Andrew J. Jenkins, Iakov Polyak, Michael J. Bearpark and Michael A. Robb

We have simulated the coupled electron and nuclear dynamics using the Ehrenfest method upon valence ionisation of modified bismethylene-adamantane (BMA) molecules where there is an electron transfer between the two p bonds. We have shown that the nuclear motion significantly affects the electron dynamics after a few fs when the electronic states involved are close in energy. We have also demonstrated how the non-stationary electronic wave packet determines the nuclear motion, more precisely the asymmetric stretching of the two p bonds, illustrating "charge-directed reactivity". Taking into account the nuclear wave packet width results in the dephasing of electron dynamics with a half-life of 8 fs; this eventually leads to the equal delocalisation of the hole density over the two methylene groups and thus symmetric bond lengths.

1 Introduction

From 2001, the emergence of tools for attosecond measurement allows the experimental study of the dynamics of electrons and nuclei in molecules, on the attosecond (1 as ¼ 10 ^{18} s) time scale.[1,2] The synthesis of attosecond pulses relies on the time–energy uncertainty principle DEDt $ ħ: collecting together coherent light sources with an energy bandwidth DE of several eV gives a pulse with duration s z ħ/DE of a few attoseconds. The broad spectral bandwidth of such short pulses leads to the coherent population of several electronic states, thus breaking the Born–Oppenheimer approximation. The system is not con ned any more to be in a single stationary electronic state but is now a superposition of electronic states, called an electronic wave packet: this superposition is non-

Department of Chemistry, Imperial College London, London SW7 2AZ, UK

† Electronic supplementary information (ESI) available: Convergence check of the spin density average amplitude with respect to the number of sampled geometries in the ensemble and comparison of potential, kinetic and total energies of the Ehrenfest trajectories in BMA[5,5] where Newton's equation of motion is integrated either with the gradient only (without the coupled-perturbed corrections) or with the Hessian-based predictor–corrector algorithm.

stationary, i.e. its probability density is time-dependent. Such electron dynamics is o en called charge migration in the literature.[3]

One key target of attosecond experiments remains the real-time observation of electron dynamics upon ionisation in molecules,[4–8] where changes in both the electronic density and the nuclear geometry are expected. Extended theoretical studies are necessary to help with the understanding of attosecond experiments. Molecular charge migration is still o en treated as a purely electronic process solving the electronic time-dependent Schr¨odinger equation at a single xed nuclear geometry:[9–14] the eff ects of the motion of the nuclei and of the natural spatial delocalisation of the nuclei due to the zero-point energy are thus both neglected. Considering a single static molecular geometry, the electronic density oscillates with a period inversely proportional to the energy gap between the populated eigenstates:

$$T = \frac{h}{E_s - E_{s'}} \quad (1)$$

The justi cation given for the xed-nuclei approximation is the diff erence in time scales of the electron and nuclear dynamics, with the electron distribution changing much faster than the nuclear geometry. Nest and Ulusoy[15] studied electron dynamics a er the partial electronic excitation of a diatomic molecule to the rst excited state (more than 3 eV above the electronic ground state). Their study suggests that the eff ect of nuclear motion is very small during the rst ten or so femtoseconds, as it takes time for the nuclei to move sufficiently to in uence the electronic superposition. Ajay and coworkers have recently shown in another diatomic molecule that the nuclear motion does not destroy the coherent electron dynamics for several tens of fs but it modulates the electronic oscillations.[16] Using the mixed quantum-classical Ehrenfest method,[17] we have previously studied molecules[18,19] where the amplitude and time scale of electron dynamics are aff ected by the nuclear motion a er only a few fs and others[18–21] where the sinusoidal oscillation in the electronic density survives for several tens of fs.

Another eff ect is that of the nuclear wave packet delocalisation: due the zero-point energy, the nuclei undergo uctuations in their positions even in the molecular ground state. The various nuclear geometries within the nuclear wave packet lead to a distribution of energy gaps and therefore of oscillation periods in the electronic density (eqn (1)). The oscillations will then dephase with time, calling into question the commonly held picture of long-lived electronic oscilla-tions at a well-de ned frequency. Using a simple analytical model, we have shown that it dephases faster when the nuclear wave packet is wider and when the diff erence of slopes of the potential energy surfaces involved is greater.[22] This eff ect is neglected in the single-geometry approximation used in most simulations until now. We have shown that the intrinsic distribution in nuclear geometries within the nuclear wave packet (sampled from a Wigner distribution) leads to the rapid dephasing of electron dynamics in para-xylene, a polycyclic norbornadiene and phenylalanine derivative cations on a few femtosecond time scale.[21,22]

With the population of an electronic wave packet, the convenient picture of a single potential energy surface is lost: the nuclei “feel” the multiple coupled potential energy surfaces and their movement is determined by the gradient of the superposition of electronic states. Experiments suggest that electronic wave packets play a chemical role. For example, Weinkauf et al. claimed that

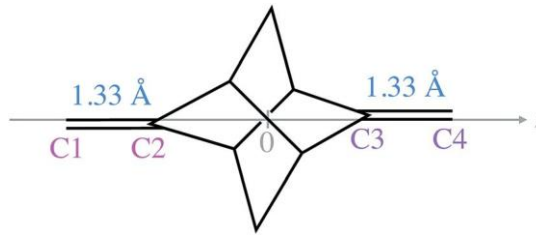

Fig. 1 Structure of the BMA[5,5] molecule: modified bismethylene-adamantane molecule where the cage consists of four connected cyclopentane (instead of cyclohexane) rings. The relevant carbon atoms are numbered. The relevant bond lengths at the equilibrium geometry of the neutral species are indicated.

fragmentation sites in small polypeptide cations were controlled by the dynamics of a superposition of quasi-degenerate electronic states.[23,24] The interpretation and simulation of such coupled electron and nuclear dynamics in molecules, o en called charge-directed reactivity in the literature, have proven to be chal-lenging. Therefore, several experimental and theoretical studies have since been [25–29]

carried out on diatomic molecules. De Vivie-Riedle extended the concept theoretically to larger molecular systems by studying in reduced dimensionality the eff ect of the initial conditions on the subsequent dynamics:[30,31] it was sug-gested to control the relative phases and amplitudes of a superposition of elec-tronic states near a conical intersection to "steer" chemical reactions and control the branching ratio of populations for instance. Using the Ehrenfest method, we have previously investigated the nature of the nuclear motion when an electronic wave packet is populated in benzene and toluene cations:[32,33] we have shown that manipulation of the details of the electronic wave packet (relative weight and phase) leads to the control of the initial nuclear motion.

In this article, we study coupled electron and nuclear dynamics upon valence ionisation of modi ed bismethylene-adamantane (BMA) molecules (Fig. 1), using our implementation of the Ehrenfest method.[17,34] The BMA cation is a model donor–linker–acceptor system where there is an electron transfer between two p bonds connected by the adamantane framework.[35,36] Vertical ionisation of the p system at the equilibrium geometry of the neutral species leads to an exact point of degeneracy between the ground and rst excited states of the cation.[37] (This does not induce electron dynamics according to eqn (1).) In a chemically modi ed BMA molecule, the vertical ionisation may take place at a geometry with a nonzero energy gap between the ground and rst excited states of the cation. This is needed to generate a non-stationary electronic wave packet. We present the theoretical methods used in Section 2. In Section 3, we study electron dynamics in modi ed BMA molecules and the diff erent eff ects of the nuclei. In Section 4, we study the nuclear motion induced by a non-stationary superposition of the electronic ground and rst excited states.

2 Methods and computational details

2.1 Initial conditions

The initial nuclear geometry is the equilibrium geometry of the neutral species, optimised using the complete active space self-consistent eld (CASSCF) method with the 4 p orbitals in the active space and a 6-31G* basis set, as implemented in

Gaussian.[34] To mimic the quantum distribution of the vibrational ground state (in the harmonic approximation), we sample 500 initial nuclear geometries and velocities from the Wigner distribution. This was done with the Newton-X program[38] using the harmonic frequencies calculated at the equilibrium geom-etry of the neutral species at the CASSCF(4,4)/6-31G* level of theory. The results depend on the number of sampled points taken into account; one must make sure convergence has been reached. We test the convergence of the results for the system studied here in the ESI (Fig. S1†).

The initial electronic wave packet is a superposition of the two lowest-energy eigenstates of the cation, j_0 and j_1,

$$J \frac{1}{4} \cos(q/2)j_0 + \sin(q/2)e^{if}j_1 \quad (2)$$

where $q/2$ determines the relative weight between the two electronic states and f the relative phase. We do not aim to simulate a speci c experiment: the relative weight $q/2$ and phase f are parameters of our simulations, the role of which is worth exploring in its own right.

2.2 Electronic structure and dynamics methods

To simulate coupled electron and nuclear dynamics, we use our CASSCF imple-mentation of the mixed quantum–classical Ehrenfest method in a development version of Gaussian.[34] The derivation and implementation details have been described previously.[17] Here, we only provide a short summary of the method.

Electron dynamics is treated quantum mechanically by integrating the elec-tronic time-dependent Schr¨odinger equation. The electronic wave packet is expanded in the con guration state function (CSF) basis generated by the active space considered; A is the vector that gathers the expansion coefficients. In practice, time is discretised and the electronic Hamiltonian H_e (in the CSF basis) is assumed to be constant over the time step. The electronic wave function at time t_n is calculated from the wave function at time $t_{n\ 1}$ using the following equation:

$$A\delta t_n P \frac{1}{4} \exp \frac{i}{\hbar} H_e \delta t_n P_{\ \delta t_n \quad t_{n\ 1} P} A\delta t_{n\ 1} P \quad (3)$$

The nuclear motion is included (if wanted) by solving the classical Newton's equation of motion:

$$\frac{dP}{dt} \frac{1}{4} V_I \quad J H_e J \quad (4)$$

with P_I the classical momentum of nucleus I. We integrate eqn (4) using the Hessian-based predictor–corrector algorithm designed by Hase and Schlegel.[17,39] A computationally cheaper alternative is to use only the gradient of the energy (without the coupled-perturbed CASSCF corrections) to integrate eqn (4).[17] We use the latter approach for the ensemble of 500 trajectories.

2.3 Analysis

To follow the evolution of the electronic wave function, its electronic spin density – that allows one to locate the unpaired electron – is computed and partitioned on the atoms (using the standard Mulliken population analysis)[40] at each step of the

simulation. This is how we monitor the hole dynamics. We also calculate the time evolution of the molecular dipole moment.

To follow the evolution of the nuclear geometry, the bond lengths of the two methylene groups (forming the two p bonds) are computed at each step of the simulation.

3 Electron dynamics and effects of the nuclei

In this section, we investigate the electron dynamics upon ionisation and the different effects of the nuclei: modi cation of the nuclear geometry, nuclear motion, and the width of the nuclear wave packet.

3.1 Chemical modi cation to engineer electron dynamics

The equilibrium geometry of the neutral BMA corresponds to a point of degen-eracy between the two lowest-energy electronic states of the cation. These two electronic states correspond to an electron being removed from the p bonds. Since the period of oscillation in the electronic density is inversely proportional to the energy gap (eqn (1)), there is no pure electron dynamics upon valence ion-isation of the p system in this molecule. A chemical modi cation is thus needed to li the degeneracy and "engineer" electron dynamics.[19] The two nuclear coordinates of the branching space that li the degeneracy are the antisymmetric stretching of the two p bonds and the deformation of the adamantane cage.[35,36] A distortion along the former coordinate leads to the adiabatic ground state of the cation having the charge localised on the longer methylene bond while the adiabatic rst excited state has the charge localised on the shorter bond. A superposition of these two states would result in a delocalised hole over the two methylene groups and not in charge migration between spatially separated parts of the molecule. We therefore choose to li the degeneracy by "chemically" deforming the adamantane cage.

The original adamantane cage consists of four connected cyclohexane rings (arranged in the "chair" con guration): each ring therefore contains 6 carbon atoms. The chemically modi ed species are obtained by altering the number of carbon atoms in the rings. By nature of the connection of the rings, two rings must share the same number of atoms. A pair of integers – each indicating the number of carbon atoms in two rings – is therefore enough to de ne the (modi ed) ada-mantane cage. Using this convention, the original BMA molecule corresponds to BMA[6,6]. In this article, we consider the following modi ed molecules: BMA[5,5] (Fig. 1), BMA[6,5] and BMA[6,7]. The energy gaps between the ground and rst excited states calculated at the CASSCF(3,4)/6-31G* level of theory are indicated in Table 1 for the modi ed molecules studied. For all these molecules, the adiabatic ground and rst excited states of the cation have a charge delocalised over the two methylene groups. An equal superposition of the two states results in a localised hole on one methylene group or the other depending on the relative phase.

3.2 Electron dynamics at single xed nuclear geometries

We start by reporting simulations of pure electron dynamics at a single xed nuclear geometry: the equilibrium geometry of the neutral species. These results are obtained with eqn (3), keeping the nuclei xed.

Table 1 Energy gap between the ground and first excited states of the cation at the equilibrium geometry of the neutral species (calculated at the CASSCF(3,4)/6-31G* level with the 4 p orbitals included in the active space) and the corresponding expected period of the oscillations (eqn (1))

Molecule	Energy gap [eV]	Period of oscillations [fs]
BMA[5,5]	0.84	4.9
BMA[6,5]	0.28	14.6
BMA[6,7]	0.11	37.0
BMA[6,6]	0.00	N

Fig. 2 shows the time evolution of the spin density upon p ionisation of BMA [5,5]. The unpaired electron initially localised on the bond C1–C2 (with a higher density on C1) – see Fig. 1 for atom numbering – migrates to the bond C3–C4: at 1.2 fs, it is delocalised over the two bonds and at 2.4 fs, it is completely localised on the other bond. It then returns to its initial position and the whole process repeats itself. Thus, the hole oscillates back and forth between the two terminal methylene groups, with a period inversely proportional to the energy gap, according to eqn (1).

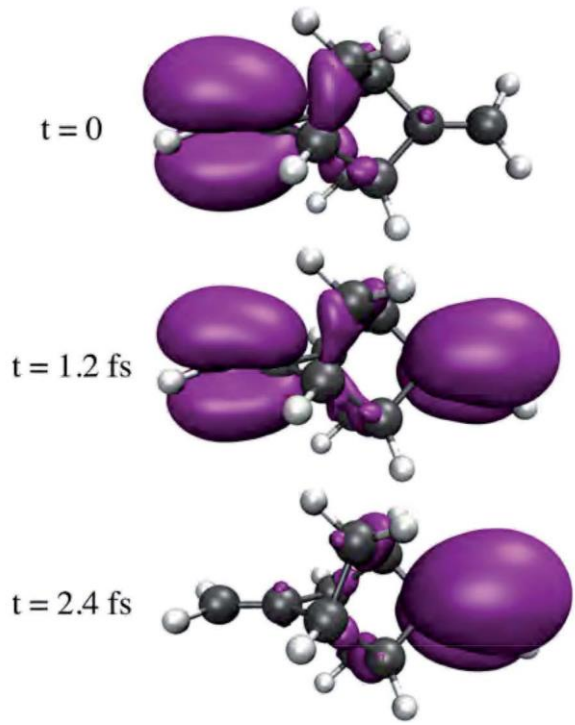

Fig. 2 Snapshots of the spin density upon ionisation of the p system in the BMA[5,5] molecule. The initial electronic wave packet is ~~ffffffi~~ ðj0 þ j1Þ. Simulation with fixed nuclei, at the equilibrium geometry of the neutral species (multimedia view available in the ESI†).

Fig. 3 shows, for the three molecules studied, the Mulliken partitioned spin densities on carbon atoms C1, C2, C3 and C4 as a function of time. The nature and amplitude of the electron dynamics are the same for the three molecules: the unpaired electron oscillates between the two terminal methylene groups, the whole time being mainly located on the outer carbon atom. The time scale of the electron dynamics is different in the three molecules, as expected, because of the different energy gaps between the two electronic states (Table 1).

We have shown that electron dynamics simulated at a single fixed nuclear geometry results in oscillations in the unpaired electron distribution through the spin density. Equivalently, the positive charge distribution can be traced in time by calculating the molecular dipole moment. Fig. 4 shows, for the three molecules studied, the time evolution of the dipole moment component along the z axis (see Fig. 1 for the molecular orientation). (The dipole components along the x and y axes are negligible.) Initially, the unpaired electron and therefore the positive charge is located on the C1–C2 bond: the component of the dipole moment along the z axis is negative and corresponds to a positive charge located approximately 1.6 Å away from the origin (here, at the centre of mass). From BMA[5,5] to BMA[6,7], the initial dipole component along the z axis is slightly more negative because the adamantane cage is bigger and the charge is therefore slightly further away from the origin. The dipole moment then oscillates between being positive and negative with the same period as the spin density, as expected. Note that electron dynamics in atoms has been probed experimentally using transient absorption spectroscopy where the electronic transition probability is proportional to the dipole moment.[41,42]

3.3 Effect of the nuclear motion

We have investigated the effect of the nuclear motion on the electron dynamics with simulations of coupled electron and nuclear dynamics started at the equilibrium geometry of the neutral species. The nuclear motion is included according to the Ehrenfest method by integrating eqn (4) with the Hessian-based predictor–corrector algorithm, with a mass-weighted step size of 0.01 amu$^{1/2}$ bohr (corresponding to a time step of approximately 0.1 fs). Fig. 5 shows, for the three molecules studied, the partitioned spin density on the left methylene group (C1 and C2) as a function of time, when the nuclei are kept fixed (solid lines) and when they are allowed to move (dashed lines) for comparison.

In BMA[5,5] (Fig. 5a), the two curves representing the oscillations in the electronic density with fixed and moving nuclei are almost exactly superimposed up to 20 fs. The period of oscillations becomes slightly shorter with time when the nuclei are allowed to move. Overall, the nuclear motion does not have a significant effect on the electron dynamics in this system, when starting from the neutral equilibrium geometry.

In BMA[6,5] (Fig. 5b), the two curves representing the electron dynamics with fixed and moving nuclei are superimposed up to approximately 5 fs. Then, the oscillations get faster when the nuclei are allowed to move: the unpaired electron comes back to its initial position at approximately $t \approx 12$ fs instead of 15 fs. Note that it does not come back completely to its initial position since the amplitude of the oscillations decreases.

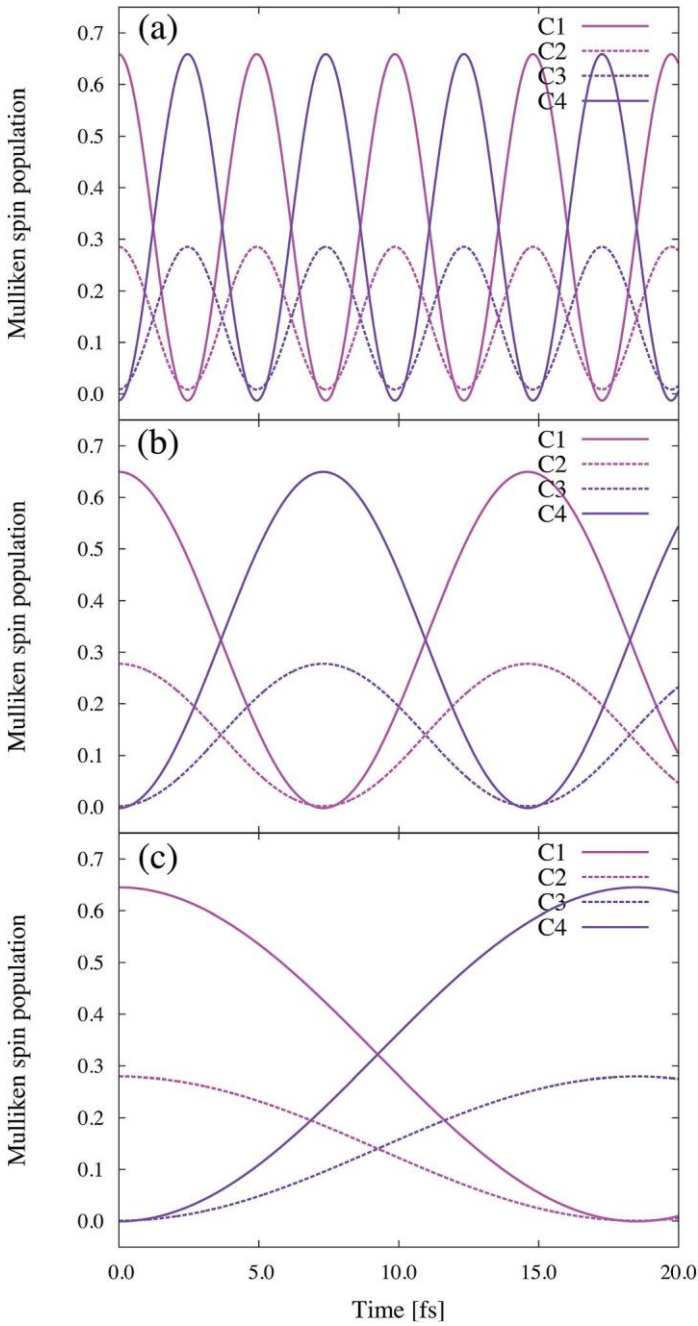

Fig. 3 Time evolution of the partitioned spin densities on the atoms of the two methylene groups, upon ionisation of the p system in the (a) BMA[5,5], (b) BMA[6,5] and (c) BMA[6,7] molecules. The initial electronic wave packet is $\frac{1}{\sqrt{2}}(j_0 + j_1)$. Simulations with fixed nuclei, at the equilibrium geometries of the neutral species. See Fig. 1 for the atom numbering.

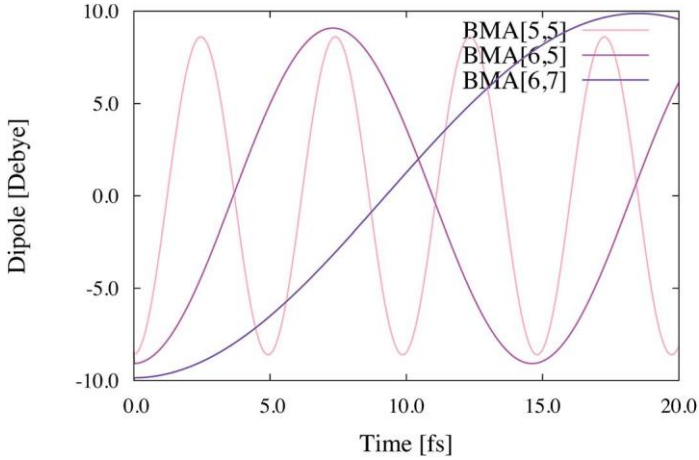

Fig. 4 Time evolution of the dipole moment along the z axis, upon ionisation of the p system in the BMA[5,5], BMA[6,5] and BMA[6,7] molecules. The initial electronic wave packet is $\frac{1}{\sqrt{2}}(\phi_0 + \phi_1)$. Simulations with fixed nuclei, at the equilibrium geometries of the neutral species. See Fig. 1 for the molecular orientation.

In BMA[6,7] (Fig. 5c), the two curves representing the electron dynamics with xed and moving nuclei are again superimposed until approximately 5 fs. Then, instead of continuing the migration to the other methylene group, the unpaired electron returns to its initial position. By the time it should have migrated completely to the other bond, it is back at the original bond, decreasing the period of oscillations by a factor of two. The amplitude of oscillations is here less than half the one with xed nuclei.

In summary: the nuclear motion can alter both the period and amplitude of the oscillations in the electronic density. The magnitude of the effect of the nuclear motion is very system-dependent. The smaller the energy gap, the slower the electron dynamics and the more signi cant the effect of the nuclear motion. This makes sense since the electron dynamics becomes slower where the two electronic states get closer in energy: there, the electron distribution changes on the same time scale as the nuclear geometry, leading to a strong coupling between the electronic and nuclear degrees of freedom.

3.4 Effect of the nuclear wave packet width

Finally, we have studied the effect of the width of the nuclear wave packet on the electron dynamics with simulations in BMA[5,5] started at 500 nuclear geometries sampled from a Wigner distribution to mimic the vibrational ground state nuclear wave packet of the neutral species. The initial electronic wave packet is $\frac{1}{\sqrt{2}}(\phi_0 + \phi_1)$. Fig. 6 shows the sum of spin density on the le methylene group (C1 2 and C2) as a function of time, for the ensemble of xed nuclear geometries simulated independently. A close look allows one to distinguish the individual oscillations that dephase with time: the different geometries in the ensemble have different energy gaps and thus result in different periods of oscillation. The

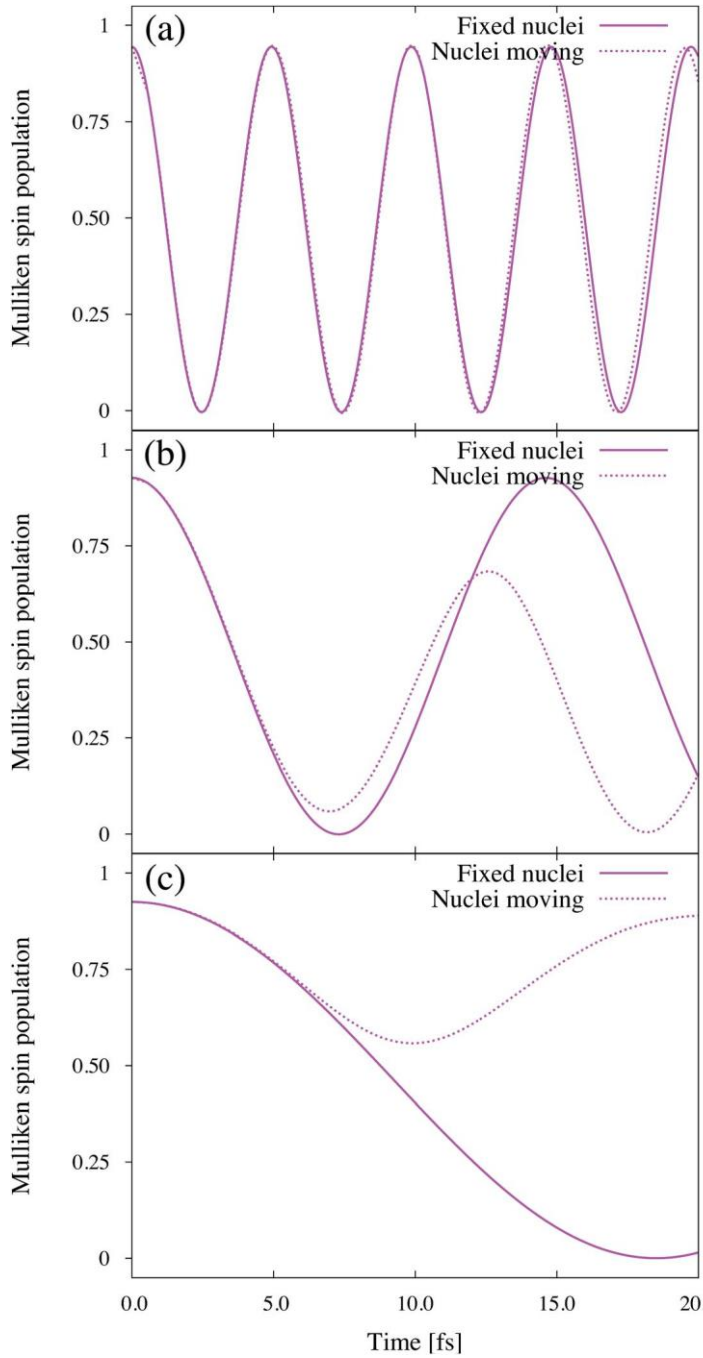

Fig. 5 Time evolution of the sum of partitioned spin densities on the atoms C1 and C2 (left methylene group), upon ionisation of the p system in the (a) BMA[5,5], (b) BMA[6,5] and (c) BMA[6,7] molecules. The initial electronic wave packet is ~~pfffffi~~ ðj0 þ j1Þ. Simulations with fixed nuclei (solid lines) and nuclei moving (dashed lines).

average oscillation amplitude is shown as a solid white line. The amplitude of the average oscillation is quickly damped with time. This results in the spin density being, on average, equally delocalised over the two methylene groups. We can extract a coherence half-life of z7 fs by tting the average spin density as explained in our previous work.[22] As mentioned above, the result depends on the number of sampled geometries taken into account. In the ESI (Fig. S1†), we present the average spin density oscillation amplitude for different sample sizes and demonstrate that 500 geometries corresponds to a converged result.

The dashed white line shows the average spin density for the ensemble when the nuclei are allowed to move according to the Ehrenfest method. Eqn (4) is integrated calculating only the gradient (with a time step of 0.05 fs) so that the 500 trajectories are computationally affordable. We have checked for a few geometries that the results obtained with the gradient only and with the Hessian-based predictor–corrector algorithm are in good agreement (see ESI†). As with xed nuclei, the average spin density oscillation is quickly damped. Surprisingly, the amplitude of the average spin density oscillation is slightly greater when the nuclei are allowed to move. A coherence half-life of z8 fs was extracted in this case. (It is not due to the energy gap distribution becoming narrower; it actually becomes wider.) It could be due to the fact that, when the nuclei move, the amplitude of the oscillations can become lower for some nuclear geometries of the ensemble (see Section 3.3 and Fig. 5). Therefore, the dephasing due to these geometries will be less important, leaving, on average, a higher amplitude oscillation.

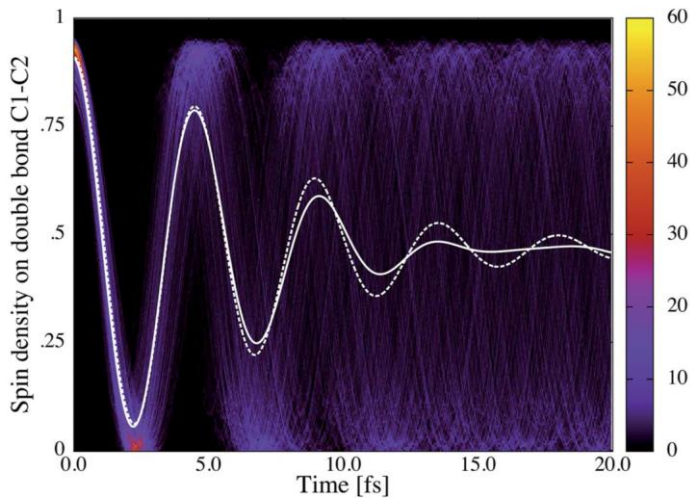

Fig. 6 Time evolution of the sum of partitioned spin densities on the atoms C1 and C2 (left methylene group), upon ionisation of the p system in the BMA[5,5] molecule, for an ensemble of 500 fixed geometries sampled from a Wigner distribution. The colour axis indicates the number of sampled trajectories in each pixel of the heat map. The solid white line indicates the spin density averaged over the ensemble of 500 sampled geometries when the nuclei are kept fixed. Also given is the spin density averaged over the ensemble of 500 trajectories (with initially sampled geometries and velocities) when the nuclei are allowed to move, indicated by the dashed white line. The initial electronic wave packet is

~~pffffffi~~ ðj0 þ j1Þ.

In summary: the effect of the nuclear wave packet width is important: it leads to a fast dephasing of the electron dynamics. In BMA[5,5], it is larger than the effect of the nuclear motion per se. The coherence half-life in the studied system here is 7–8 fs which is longer than in other systems we have studied (4 fs in the para-xylene cation[22] and 2 fs in the phenylalanine deriv-ative cations[21]). The relevant properties for the dephasing time scale are the width of the nuclear wave packet and the relative slopes of the involved potential energy surfaces:[22] a narrow wave packet and parallel potential energy surfaces result in a narrow energy gap distribution and therefore a slow dephasing. A possible explanation for the "long" coherence half-life in BMA [5,5] is the rigid structure of the cage, which limits the nuclear wave packet width and therefore the energy gap distribution width. Because of the rela-tively "long" coherence half-life and because of the short period of oscillations (4.9 fs), we observe several oscillations in the electronic density before dephasing occurs.

4 Nuclear motion and electronic coherent control

In this section, we analyse the nuclear motion upon ionisation induced by a single electronic eigenstate and by a superposition of them to investigate the differ-ences. We are particularly interested in the evolution of the bond lengths of the two terminal methylene groups with time.

4.1 Nuclear motion induced by a single stationary adiabatic electronic state

For reference, we report simulations started at the equilibrium geometry of the neutral species with only the electronic ground state populated. Upon pop-ulation of the adiabatic ground state of the cation, the unpaired electron is delocalised over the two methylene groups (like in the centre snapshot of Fig. 2). It does not evolve signi cantly with time (not shown): there is no pure electron dynamics since a single stationary adiabatic state is initially popu-lated. (Change in the electronic distribution due to the nuclear motion – called charge transfer in the literature – could happen on a longer time scale.) In Fig. 7, we present, for the BMA[5,5] molecule, the time evolution of the average and difference in bond lengths of the two methylene groups. The results for the BMA[6,5] and BMA[6,7] molecules are almost identical (not shown). Initially, the two C1 C2 and C3 C4 bond lengths are equal to 1.33 Å (a typical value for a carbon double bond). We observe that the average bond length stretches to 1.42 Å and shortens back to the initial value in approximately 20 fs. The stretching is expected since an electron has been removed from a bonding π orbital. Note that the frequency of C]C stretching is typically in the range of 1640–1680 cm^{-1}, which corresponds to a period of vibration of approximately 20 fs. Our simulations are in agreement with this value. An important point is that, here, the difference in bond lengths between the two terminal methylene groups is null: the stretching is symmetric, as expected since the unpaired electron is equally, i.e. symmetrically, delocalised over the two methylene groups.

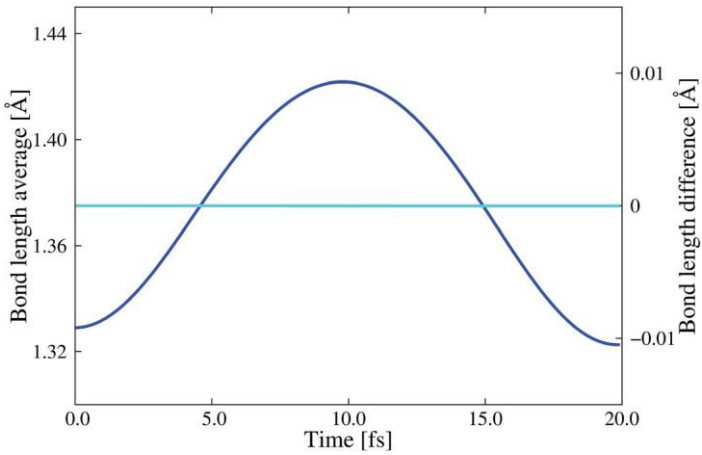

Fig. 7 Time evolution of the bond lengths of the two methylene groups (average length of the C1–C2 and C3–C4 bonds in blue with the left y axis and difference in cyan with the right y axis), upon ionisation of the p system in the BMA[5,5] molecule. The initial electronic state is the ground state j0.

4.2 Nuclear motion induced by a non-stationary superposition of electronic states

We now analyse the nuclear motion induced when the electronic wave packet $\frac{1}{\sqrt{2}}(|0\rangle + |1\rangle)$ is initially populated and we investigate how it differs from the nuclear motion induced by a stationary adiabatic electronic state (Section 4.1). Fig. 8 shows, for the three molecules studied, the time evolution of the average and difference in bond lengths of the two methylene groups in this case. Note that the scale for the bond length difference is the same as for the bond length average except in Fig. 8a for which it is 5 times smaller. The black dashed lines remind the reader of the oscillations in the electronic density (with nuclei moving) from Fig. 5.

In BMA[5,5] (Fig. 8a), the average bond length evolves in a similar way to the case of dynamics induced by the electronic ground state solely (Fig. 7): it stretches and vibrates with a period of 20 fs. The difference in bond lengths between the two methylene groups, however, differs from 0: the stretching is asymmetric. More precisely, we observe oscillations in the difference in bond lengths, the period of which matches the period of the oscillations in the spin density (indi-cated by the black dashed line). Initially, the electronic density is asymmetric with the unpaired electron (or positive charge) located on the C1–C2 bond; the nuclei thus react asymmetrically i.e. the C1–C2 bond stretches more than the C3–C4 bond and the difference in bond length (C3–C4)–(C1–C2) becomes negative. As the unpaired electron migrates to the C3–C4 bond, the process will reverse and the C3–C4 bond will stretch more than the C1–C2 bond. Note that it takes a few fs for the nuclear motion to reverse since it has acquired some kinetic energy. Note that the bond length difference does not just oscillate around 0; there is an overall slower evolution. The oscillations in the bond length difference is an illustration of “charge-directed reactivity”: the nuclear and electron dynamics are

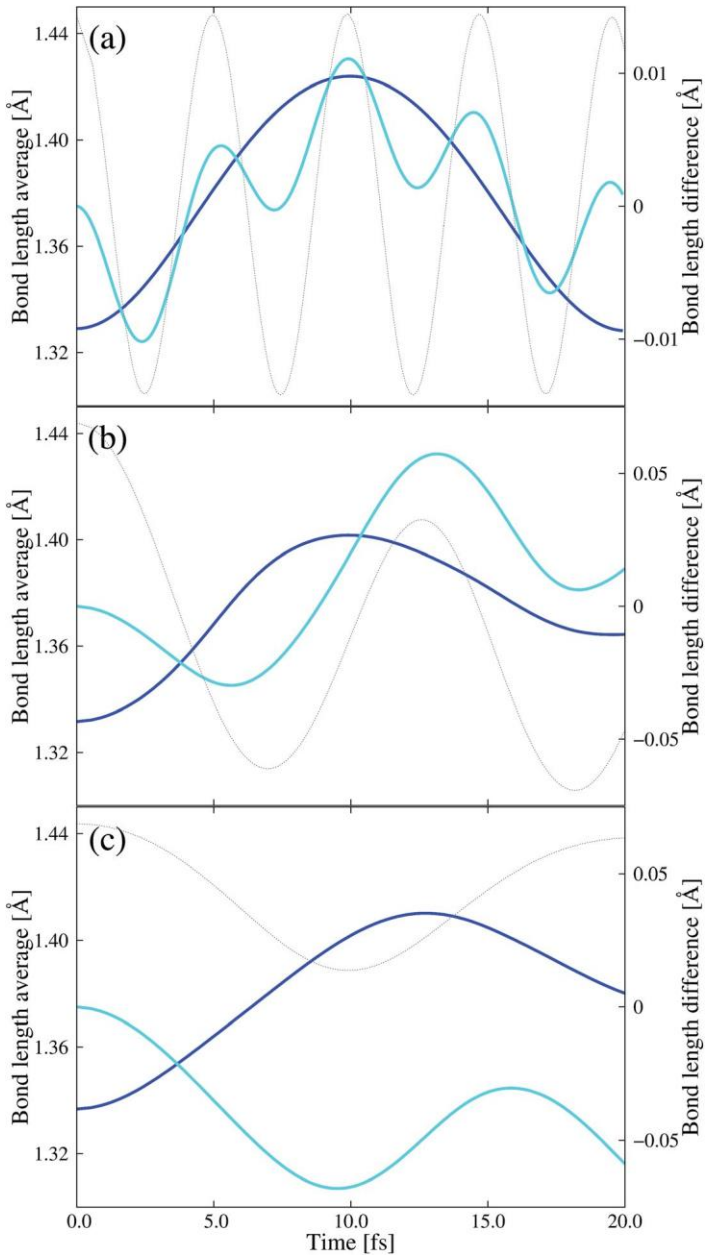

Fig. 8 Time evolution of the bond lengths of the two methylene groups (average length of the C1–C2 and C3–C4 bonds in blue with the left y axis and difference (C3–C4)–(C1–C2) in cyan with the right y axis), upon ionisation of the p system in the (a) BMA[5,5], (b) BMA[6,5] and (c) BMA[6,7] molecules. The initial electronic wave packet is $\frac{1}{2}(\psi_0 + \psi_1)$. The scale for the bond length difference is the same as for the bond length average except for BMA[5,5] for which it is 5 times smaller. The black dashed lines remind the reader of the oscillations in the electronic density from Fig. 5.

asynchronous, the nuclei always trying to adapt to the time-dependent electronic distribution.

We observe similar behaviour in the bond length difference for BMA[6,5] (Fig. 8b) and BMA[6,7] (Fig. 8c). Note that in these two molecules, the difference in bond length reaches larger values (the scale being 5 times larger). In these cations the periods of the oscillations in the electronic density are longer, so the bonds stretch asymmetrically for longer. Here, the larger difference in bond lengths affects the time evolution of the average bond length which is not bell-shaped any more.

In summary: the superposition of the two lowest-energy electronic states induces an asymmetric stretching of the two terminal methylene bonds (while each electronic state populated individually induces a symmetric stretching). This is because of the unpaired electron not being equally delocalised over the two terminal groups when a superposition of electronic states is populated. The oscillations with time of the electronic density result in oscillations in the nuclear motion as well, the nuclei continuously trying to adapt to the time-dependent electronic distribution.

To illustrate the "charge-directed reactivity" idea further, we have simulated coupled electron and nuclear dynamics in the BMA[6,5] cation, induced by the electronic wave packets $\frac{1}{\sqrt{2}}(\psi_0 + e^{i\phi}\psi_1)$ with the different relative phases $\phi = 0, 90, 180$ and 270. The case of $\phi = 0$ corresponds to the equal in-phase superposition as in Fig. 5b and 8b. Fig. 9 shows, for the different initial electronic wave packets, the time evolution of the partitioned spin density on the left methylene group (C1 and C2). The initial relative phase determines the initial position of the unpaired electron: the latter is localised on the C1–C2 bond with $\phi = 0$ (as in Fig. 5b), on the C3–C4 bond with $\phi = 180$, and delocalised over the two bonds with

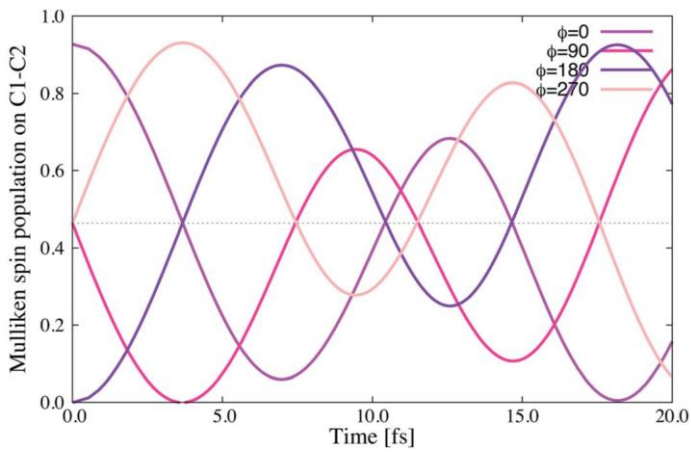

Fig. 9 Time evolution of the sum of partitioned spin densities on the atoms C1 and C2 (left methylene group), upon ionisation of the p system in the BMA[6,5] molecule. The initial electronic wave packets are $\frac{1}{\sqrt{2}}(\psi_0 + e^{i\phi}\psi_1)$ with different relative phases $\phi = 0, 90, 180$ and 270. Simulations with nuclei moving. The dotted horizontal line at $y = 0.46$ indicates the spin density value when the unpaired electron is equally delocalised over the two terminal methylene groups.

f ¼ 90 and 270. The spin density then oscillates with time between the two methylene groups. As the initial phase determines the value of the oscillation at t ¼ 0, it can be seen as a shi of the time axis. The oscillations are not perfect sinusoids: the amplitude and period vary with time because of the nuclear motion (see Section 3.3). Note that the curves for f ¼ 0 and 180, and for f ¼ 90 and 270, are symmetric with respect to y ¼ 0.46 (the value corresponding to the spin density equally delocalised over the two methylene groups).

Fig. 10 shows, for the different initial electronic wave packets, the time evolution of the bond length difference. We observe again oscillations in the bond length differences that follow the oscillations in the spin densities (Fig. 9). We notice that the nuclear motions induced by f ¼ 0 and 180, and by 90 and 270 are symmetric with respect to y ¼ 0 (the value corresponding to equal C1–C2 and C3– C4 bond lengths). Indeed, with f ¼ 180, the C3–C4 bond initially stretches more than C1–C2 since the unpaired electron is this time localised on C3–C4 at t ¼ 0. Besides, the absolute difference in bond lengths is initially lower with the relative phases f ¼ 90 and 270 than with 0 and 180: the unpaired electron being equally delocalised over the two methylene groups at t ¼ 0 with f ¼ 90 or 270, the induced nuclear motions are symmetric stretching. With time, as the unpaired electron migrates to one of the two bonds, it then induces an asymmetric stretching. Note that the unpaired electron initially stays more localised on one bond for 8 fs (zhalf a period) with f ¼ 90 or 270 before migrating to the other bond, while it migrates to the other bond a er only 4 fs (za quarter of period) with f ¼ 0 or 180 (because of the "shi " of the time axis). As a result, the (absolute) difference in

bond lengths has the time tq become greater with f ¼ 90 or 270: 0.07 A reached at z9.0 fs compared to 0.03 A reached at z5.6 fs.

In summary: we have illustrated how by manipulating the composition of the initial electronic wave packet (relative weight and phase), one can manipulate the initial nuclear motion, i.e. which bond stretches more (if any) and by how much.

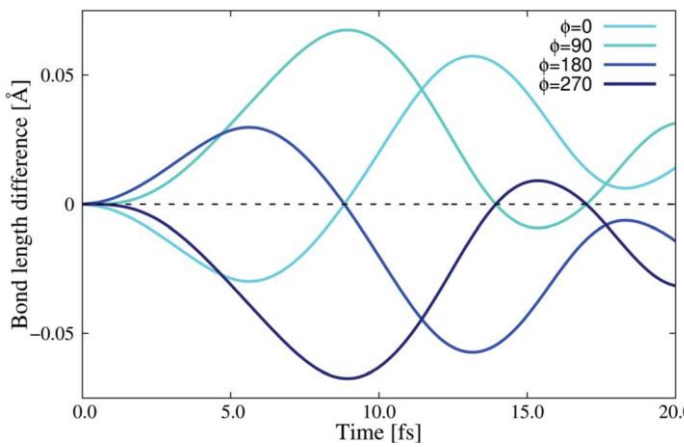

Fig. 10 Time evolution of the bond length difference between the two methylene groups (C3–C4)–(C1–C2), upon ionisation of the p system in the BMA[6,5] molecule. The initial

electronic wave packets are ~~pffffffi~~ðj0 þ e j1Þ with different relative phases f ¼ 0, 90, 180 2 and 270 . Simulations with nuclei moving.

4.3 Nuclear motion with an ensemble of trajectories to mimic the nuclear wave packet width

Finally, we have studied the effect of the width of the nuclear wave packet on the nuclear motion with simulations in BMA[5,5] started at 500 sampled nuclear geometries and velocities (see Section 3.4). The initial electronic wave packet is

$\frac{1}{\sqrt{2}}(|0\rangle + |1\rangle)$. Fig. 11 shows the bond length average as a function of time, for the ensemble of trajectories simulated independently. The dashed white line indicates the average value of the ensemble. The initial width of the distribution is characterised by a standard deviation of 0.04 Å. The ensemble of trajectories undergoes a stretching of the average bond length to 1.42 Å with a period of vibration of 20 fs, as the single "un-sampled" trajectory started at the neutral equilibrium geometry with no kinetic energy (Fig. 8a). Note that the time evolution of the average length of the C1–C2 and C3–C4 bonds does not result from the electron dynamics of a non-stationary electronic wave packet; it was also observed with the stationary electronic ground state initially populated (Fig. 7). Therefore, we do not expect a dephasing of this vibrational motion with time.

Fig. 12 shows the time evolution of the difference in bond lengths of the two methylene groups, averaged over the ensemble of 500 trajectories. The black dashed line reminds the reader of the oscillations in the electronic density (averaged over the 500 trajectories) from Fig. 6. The bond length difference oscillates with time, as in Fig. 8a initially; then, the oscillations are damped. The oscillations look to be on top of an overall slower evolution, as in Fig. 8a. To help with the interpretation of the damping of the oscillations, Fig. 13 shows the time derivative of the difference in bond lengths of the two methylene groups, averaged over the ensemble of 500

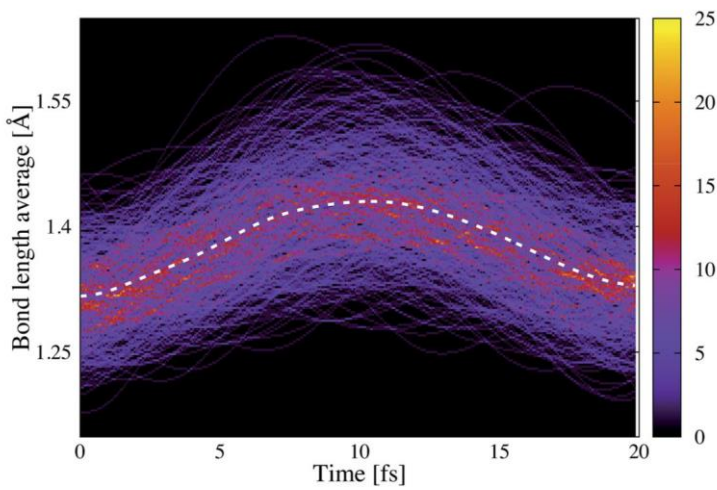

Fig. 11 Time evolution of the average bond length of the C1–C2 and C3–C4 bonds, upon ionisation of the p system in the BMA[5,5] molecule, for an ensemble of 500 geometries and velocities sampled from a Wigner distribution. The colour axis indicates the number of sampled trajectories in each pixel of the heat map. The dashed white line indicates the average value of the ensemble. The initial electronic wave packet is $\frac{1}{\sqrt{2}}(|0\rangle + |1\rangle)$.

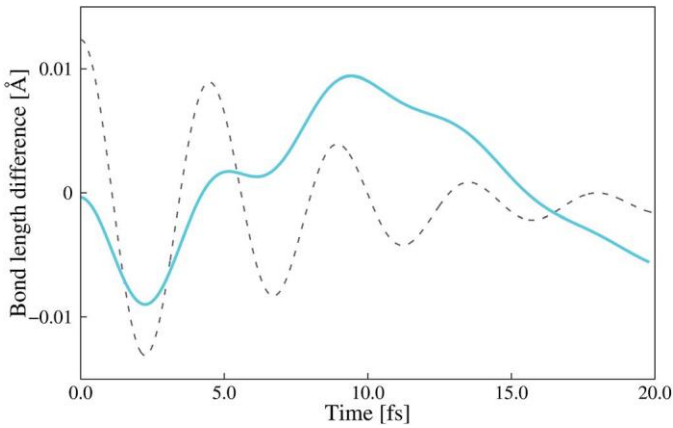

Fig. 12 Time evolution of the difference in bond lengths of the two methylene groups (C3–C4)–(C1–C2), averaged over the ensemble of 500 trajectories (with sampled geometries and velocities), upon ionisation of the p system in BMA[5,5]. The initial electronic wave packet is $\frac{1}{\sqrt{2}}(|j_0\rangle + |j_1\rangle)$. The black dashed lines remind the reader of the 2 oscillations in the electronic density from Fig. 6.

trajectories. Similarly, the black dashed line is the time derivative of the oscillations in the electronic density (averaged over the 500 trajectories). We clearly see that, when taking into account an ensemble of trajectories to represent the nuclear wave packet, the oscillations in the bond length difference are damped just as the oscillations in the spin density dephase.

In summary: the effect of the nuclear wave packet width is again important. As the electron dynamics dephase and the unpaired electron becomes equally delocalised over the two methylene groups, the asymmetry in the stretching of the two p bonds disappears.

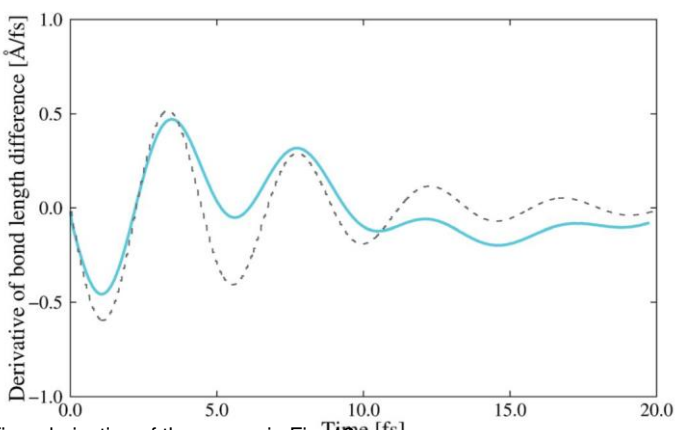

Fig. 13 Time derivative of the curves in Fig. 12.

5 Conclusion

In this article, we have studied the electron and nuclear dynamics upon valence ionisation of the p system in three modi ed BMA molecules. Chemical modi - cation to the BMA molecule was necessary to li the energy gap between the ground and rst excited cationic states at the neutral equilibrium geometry and “engineer” electron dynamics. Using the Ehrenfest method, we have studied the eff ect of the nuclear motion on the electron dynamics. The latter is signi cant in molecules where the energy gap is small (lower than 0.3 eV) since the electron dynamics slows down to the time scale of the nuclear motion. Another important eff ect is that of the width of the nuclear wave packet. The natural distribution of geometries within the nuclear wave packet leads to the fast dephasing of electron dynamics. In BMA[5,5], we have extracted a coherence half-life of 7 fs which, with the short period of oscillations, leaves enough time for several oscillations in the electronic density before dephasing occurs. Surprisingly, the nuclear motion helps maintaining the coherence for slightly longer by damping the oscillations at some distorted geometries that led to dephasing.

Ionisation of the p system leads to an overall stretching of the two carbon double bonds. We have shown that the population of a single adiabatic state results in a symmetric stretching. On the other hand, the population of a super-position of the ground and rst excited state breaks the symmetry by localising the unpaired electron on one methylene group and leads to an asymmetric stretching. This is a demonstration of “charge-directed reactivity”. As the unpaired electron oscillates from one methylene group to the other, the diff er-ence in bond length of the two bonds oscillates with the same period. The nuclear geometry is continuously trying to adapt to the time-dependent electronic density. By manipulating the composition of the superposition of states, for instance the relative phase, one can manipulate the asymmetry of the nuclear motion, i.e. which bond stretches more and by how much. When taking into account an ensemble of sampled trajectories, the asymmetry in stretching eventually disap-pears as the dephasing of electron dynamics leads to an equal delocalisation of the unpaired electron on the two methylene groups.

Acknowledgements

This work was supported by UK-EPSRC Grant EP/I032517/1. All calculations were run using the Imperial College High Performance Computing service.

References

1 P. M. Paul, E. S. Toma, P. Breger, G. Mullot, F. Aug´e, P. Balcou, H. G. Muller and P. Agostini, Science, 2001, 292, 1689–1692.
2 M. Hentschel, R. Kienberger, C. Spielmann, G. A. Reider, N. Milosevic, T. Brabec, P. Corkum, U. Heinzmann, M. Drescher and F. Krausz, Nature, 2001, 414, 509–513.
3 J. Breidbach and L. S. Cederbaum, J. Chem. Phys., 2003, 118, 3983–3996.
4 A. I. Kuleff and L. S. Cederbaum, Phys. Rev. Lett., 2011, 106, 053001.
5 L. Belshaw, F. Calegari, M. J. Duffy, A. Trabattoni, L. Poletto, M. Nisoli and J. B. Greenwood, J. Phys. Chem. Lett., 2012, 3, 3751–3754.

6 J. Leeuwenburgh, B. Cooper, V. Averbukh, J. P. Marangos and M. Ivanov, Phys. Rev. Lett., 2013, 111, 123002.
7 F. Calegari, D. Ayuso, A. Trabattoni, L. Belshaw, S. De Camillis, S. Anumula, F. Frassetto, L. Poletto, A. Palacios, P. Decleva, J. B. Greenwood, F. Mart´ın and M. Nisoli, Science, 2014, 346, 336–339.
8 S. R. Leone, C. W. McCurdy, J. Burgdorfer, L. S. Cederbaum, Z. Chang, N. Dudovich, J. Feist, C. H. Greene, M. Ivanov, R. Kienberger, U. Keller, M. F. Kling, Z.-H. Loh, T. Pfeifer, A. N. Pfeiffer, R. Santra, K. Schafer, A. Stolow, U. Thumm and M. J. J. Vrakking, Nat. Photonics, 2014, 8, 162–166.
9 F. Remacle and R. Levine, Z. Phys. Chem., 2007, 221, 647–661.
10 A. I. Kuleff and L. S. Cederbaum, Chem. Phys., 2007, 338, 320–328.
11 S. Lunnemann,¨ A. I. Kuleff and L. S. Cederbaum, Chem. Phys. Lett., 2008, 450, 232–235.
12 S. Lunnemann,¨ A. I. Kuleff and L. S. Cederbaum, J. Chem. Phys., 2008, 129, 104305.
13 G. Periyasamy, R. Levine and F. Remacle, Chem. Phys., 2009, 366, 129–138.
14 A. I. Kuleff, S. Lunnemann¨ and L. S. Cederbaum, J. Phys. Chem. A, 2010, 114, 8676–8679.
15 I. S. Ulusoy and M. Nest, J. Phys. Chem. A, 2012, 116, 11107–11110.
16 J. Ajay, J. Smydke, F. Remacle and R. D. Levine, J. Phys. Chem. A, 2016, 120, 3335–3342.
17 M. Vacher, D. Mendive-Tapia, M. J. Bearpark and M. A. Robb, Theor. Chem. Acc., 2014, 133, 1505.
18 D. Mendive-Tapia, M. Vacher, M. J. Bearpark and M. A. Robb, J. Chem. Phys., 2013, 139, 044110.
19 M. Vacher, D. Mendive-Tapia, M. J. Bearpark and M. A. Robb, J. Chem. Phys., 2015, 142, 094105.
20 M. Vacher, M. J. Bearpark and M. A. Robb, J. Chem. Phys., 2014, 140, 201102.
21 A. J. Jenkins, M. Vacher, M. J. Bearpark and M. A. Robb, J. Chem. Phys., 2016, 144, 104110.
22 M. Vacher, L. Steinberg, A. J. Jenkins, M. J. Bearpark and M. A. Robb, Phys. Rev. A, 2015, 92, 040502.
23 F. Remacle, R. D. Levine, E. W. Schlag and R. Weinkauf, J. Phys. Chem. A, 1999, 103, 10149–10158.
24 R. Weinkauf, E. W. Schlag, T. J. Martinez and R. D. Levine, J. Phys. Chem. A, 1997, 101, 7702–7710.
25 A. D. Bandrauk, S. Chelkowski and H. S. Nguyen, Int. J. Quantum Chem., 2004, 100, 834–844.
26 V. Roudnev, B. D. Esry and I. Ben-Itzhak, Phys. Rev. Lett., 2004, 93, 163601.
27 M. F. Kling, C. Siedschlag, A. J. Verhoef, J. I. Khan, M. Schultze, T. Uphues, Y. Ni, M. Uiberacker, M. Drescher, F. Krausz and M. J. J. Vrakking, Science, 2006, 312, 246–248.
28 D. Geppert, P. von den Hoff and R. de Vivie-Riedle, J. Phys. B: At., Mol. Opt. Phys., 2008, 41, 074006.
29 P. von den Hoff, I. Znakovskaya, M. Kling and R. de Vivie-Riedle, Chem. Phys., 2009, 366, 139–147.
30 A. Hofmann and R. de Vivie-Riedle, J. Chem. Phys., 2000, 112, 5054–5059.
31 P. v. d. Hoff, S. Thallmair, M. Kowalewski, R. Siemering and R. de Vivie-Riedle, Phys. Chem. Chem. Phys., 2012, 14, 14460–14485.

32 J. Meisner, M. Vacher, M. J. Bearpark and M. A. Robb, J. Chem. Theory Comput., 2015, 11, 3115–3122.
33 M. Vacher, J. Meisner, D. Mendive-Tapia, M. J. Bearpark and M. A. Robb, J. Phys. Chem. A, 2015, 119, 5165–5172.
34 M. J. Frisch, G. W. Trucks, H. B. Schlegel, G. E. Scuseria, M. A. Robb, J. R. Cheeseman, G. Scalmani, V. Barone, B. Mennucci, G. A. Petersson, H. Nakatsuji, M. Caricato, X. Li, H. P. Hratchian, J. Bloino, B. G. Janesko, A. F. Izmaylov, A. Marenich, F. Lipparini, G. Zheng, J. L. Sonnenberg, W. Liang, M. Hada, M. Ehara, K. Toyota, R. Fukuda, J. Hasegawa, M. Ishida, T. Nakajima, Y. Honda, O. Kitao, H. Nakai, T. Vreven, K. Throssell, J. A. Montgomery, J. E. Peralta, F. Ogliaro, M. Bearpark, J. J. Heyd, E. Brothers, K. N. Kudin, V. N. Staroverov, T. Keith, R. Kobayashi, J. Normand, K. Raghavachari, A. Rendell, J. C. Burant, S. S. Iyengar, J. Tomasi, M. Cossi, N. Rega, J. M. Millam, M. Klene, J. E. Knox, J. B. Cross, V. Bakken, C. Adamo, J. Jaramillo, R. Gomperts, R. E. Stratmann, O. Yazyev, A. J. Austin, R. Cammi, C. Pomelli, J. W. Ochterski, R. L. Martin, K. Morokuma, V. G. Zakrzewski, G. A. Voth, P. Salvador, J. J. Dannenberg, S. Dapprich, P. V. Parandekar, N. J. Mayhall, A. D. Daniels, O. Farkas, J. B. Foresman, J. V. Ortiz, J. Cioslowski and D. J. Fox, Gaussian Development Version, Revision I.04+, Gaussian, Inc., Wallingford CT, 2014.
35 L. Blancafort, F. Jolibois, M. Olivucci and M. A. Robb, J. Am. Chem. Soc., 2001, 123, 722–732.
36 L. Blancafort, P. Hunt and M. A. Robb, J. Am. Chem. Soc., 2005, 127, 3391–3399.
37 I. Tavernelli, J. Phys. Chem. A, 2007, 111, 13528–13536.
38 M. Barbatti, G. Granucci, H. Lischka, M. Persico and M. Ruckenbauer, Newton-X: a package for Newtonian dynamics close to the crossing seam, version 0.11b, www.univie.ac.at/newtonx, 2006.
39 J. M. Millam, V. Bakken, W. Chen, W. L. Hase and H. B. Schlegel, J. Chem. Phys., 1999, 111, 3800–3805.
40 R. S. Mulliken, J. Chem. Phys., 1955, 23, 1833–1840.
41 E. Goulielmakis, Z.-H. Loh, A. Wirth, R. Santra, N. Rohringer, V. S. Yakovlev, S. Zherebtsov, T. Pfeifer, A. M. Azzeer, M. F. Kling, S. R. Leone and F. Krausz, Nature, 2010, 466, 739–743.
42 A. R. Beck, B. Bernhardt, E. R. Warrick, M. Wu, S. Chen, M. B. Gaarde, K. J. Schafer, D. M. Neumark and S. R. Leone, New J. Phys., 2014, 16, 113016.